Chapter 287

Lanthanide Luminescence: From a Mystery to Rationalization, Understanding, and Applications

Jean-Claude G. Bünzli[1]

Institute of Chemical Sciences and Engineering, Swiss Federal Institute of Technology Lausanne (EPFL), Lausanne, Switzerland

Haimen Institute of Science and Technology, Hong Kong Baptist University, Haimen, PR China

[1]*Corresponding author: e-mail: jean-claude.bunzli@epfl.ch*

Chapter Outline

Handbook on the Physics and Chemistry of Rare Earths, Vol. 50. http://dx.doi.org/10.1016/bs.hpcre.2016.08.003

1 INTRODUCTION

A search for lanthanide luminescence and associated terms in bibliographic databases or Web search engines typically returns tens of thousands of articles, pointing to the attractiveness of the field [1]. As a matter of fact, lanthanide luminescence is at the heart of applications as diverse as lighting, telecommunications, security marking, lasers, luminescent molecular thermometers, barcoding, or immunoassays. The subject is fascinating and has always accompanied the development of lanthanide science and technology, from the early discovery of the 4f elements to present high-technology applications. A quick look into market statistics and estimates shows that light-emitting materials (phosphors) and pigments represent the second most important application of rare earths with respect to commercial value of the rare-earth oxides needed for their production (share: about 30%), just behind permanent magnets (about 40%). However, tonnage-wise luminescent materials represent an estimated market share of only about 8% of the total rare earths consumed annually. The large added value of luminescent phosphors, probes, and materials partly explains the enthusiasm research groups are coming up with in looking for new and better materials, in addition to fascination for light emission.

In this perspective essay, we highlight the various facets of light emission by lanthanide compounds with special emphasis on historical developments, understanding the underlying mechanisms, and presentation of leading applications. The topic is vast so that only salient features will be depicted [2]. It is noteworthy that the handbook series has published to date about two dozen of chapters dealing with or including description of light emission by rare-earth inorganic compounds or chelates; they focus on photoluminescence [3–6], laser effect and spectroscopy [7–9], thermoluminescence [10], long-persistent luminescence [11], and photoemission [12–14]. These reviews are sometimes combined with theoretical modeling and/or describe applications such as sensing [15,16], drug delivery [17], luminescent nanomaterials [18], phosphors for light-emitting diodes (LEDs) [19], luminescent thermometry [20], solar energy conversion [21], optical refrigeration [22], or quantum information processing [23]. Furthermore, several chapters are dedicated to the theory of excited states and intensities of f–f transitions [9,24–26].

Before starting, it may be useful to briefly define luminescence. Emission of light by chemical compounds or materials stems from two different mechanisms: (i) incandescence, or black-body emission, which does not depend on the chemical nature of the material but only on its temperature, and (ii) luminescence or "cold light emission" [27] involving quantified energy levels in the sample. Luminescence can be excited in different ways and specific terms are used accordingly. For instance, photoluminescence results when the sample is irradiated with photons; electroluminescence is produced upon excitation of the sample in an electric discharge or in an electric field; cathodoluminescence is

generated when the sample is subjected to an electron flux; chemiluminescence (bioluminescence) arises from the energy released by a chemical (biological) reaction; thermoluminescence is consecutive to heating of the sample, liberating energy trapped in defects; mechanoluminescence is observed upon mechanical stress imposed to the sample.

Regarding nomenclature, "luminescence" is a generic term for quantified emission of light. If the two emitting and receiving levels have the same spin, the process is spin allowed, fast, and is termed "fluorescence." When the emitting level has different spin than the receiving level, then the process is spin forbidden, therefore, much slower, and is called "phosphorescence."

Most trivalent lanthanides ions are luminescent, baring La^{III} and Lu^{III}, and, except for Ce^{III}, the corresponding transitions mainly occur as electronic rearrangement within the 4f shell (f–f transitions). Electric dipole f–f transitions are forbidden by Laporte's selection rule while magnetic-dipole transitions are allowed, but faint. Selection rules are somewhat relaxed by orbital mixing with various functions, due to spin-orbit coupling, vibronic coupling, J-mixing, or mixing with ligand orbitals, but in any case the oscillator strengths remain small. Some Ln^{III} ions are phosphorescent (e.g., Eu^{III}, Tb^{III}), others are fluorescent (e.g., Ho^{III}, Yb^{III}), while many of them are both fluorescent and phosphorescent (e.g., Pr^{III}, Nd^{III}). Interconfigurational, e.g., f↔d and charge-transfer (CT), transitions are allowed. The three types of transitions are discussed in more details in Section 3.2.

2 EARLY APPLICATIONS AND THE DISCOVERY OF RARE-EARTH ELEMENTS

The first two commercial applications of lanthanides were connected to lighting and developed by the Austrian scientist and entrepreneur Carl Auer von Welsbach. The first patent filed by Auer in 1885 described a gas mantle made of a platinum grid coated with a mixture of magnesium oxide (60%), lanthanum oxide (20%), and yttrium oxide (20%); the mantle was very fragile and its emission was greenish so that the company started by Auer in 1887 went bankrupt in 1889. Not discouraged by this initial failure, Auer found that thorium oxide was a better material than magnesium oxide, and in 1891 he was granted a patent for what is known as the Auer mantle (or Auer light): a small cotton bag impregnated with a mixture of 99% thorium nitrate and 1% cerium nitrate; upon contact with the flame, the cotton burns and the nitrates are converted into oxides, yielding a bright white emission. The success was immediate and the mantles and their subsequent improved versions were ubiquitous in gas lighting until the mid-1930s. They can still be bought today; for instance for camping lamps, thorium radioactivity being considered to lie within safe regulatory limits. The second invention is a pyrophoric alloy made of 70% cerium and 30% iron (ferrocerium) that Auer patented in 1903

and used for producing flint stones for various kinds of lighters; this material, called Mischmetal, is still in use today and exists in many different versions, some of them containing rare earths only.

The invention of the spectroscope by Joseph von Fraunhofer in 1814 provided a valuable tool for studying the solar spectrum and for identifying new elements. Robert Bunsen observed sharp emission lines from rare-earth salts in the mid-1860s, and since then many scientists, including Sir William Crookes, turned to this method to detect new elements in several materials, including rare earth-containing minerals. At the beginning of the 20th century, there was a great confusion among specialists about rare-earth elements. Although most of the latter had been chemically separated and identified (at least as their oxides), the study of optical properties, such as absorption spectra, spark spectra in which emission of light is induced by submitting the sample to electric sparks, cathodoluminescence and phosphorescence spectra, generated confusing data. Given the sensitivity of the techniques and the fact that most samples were not of the highest purity, spectroscopists were recording "anomalous" lines and were therefore speculating on the presence of new elements. For instance, Sir William Crookes noted that different yttrium samples would give the same spark spectra, but different phosphorescence spectra, so that he tried to conciliate these two contradictory experiments by the concept of "meta-elements" in which an "element" with a constant spark spectrum is composed of distinct atoms having different phosphorescence spectra, much as elements are made of different isotopes. Thanks to a painstaking detailed investigation by Georges Urbain who purified series of samples until spectroscopic properties became invariant, the "meta-elements" were finally shown to correspond to known lanthanides. The rigorous protocol followed in Urbain's investigation allowed him to discover two new elements, lutetium and hafnium (that he initially called celtium) [28]. Another benefit of this research was the observation that even minute quantities of a luminescent ion such as Eu^{III} embedded into an inorganic matrix (e.g., gadolinium oxide, alumina, calcium oxide) give intense emission lines, while the pure product is often poorly or non luminescent. It was established that the best doping concentration is around 0.5–1%; in a way this may be considered as the start of the research on phosphors that led to the unique Y_2O_3:Eu^{III} red-emitting material still in use today.

However, everything was not yet solved and some doubts remained as to the presence of one or two elements in some samples since diluting a luminescent compound in different matrices gave different spectra. In particular for Eu^{III}, the intensity ratio I(613 nm)/I(593 nm)—in fact $I(^5D_0 \rightarrow {}^7F_2)/I(^5D_0 \rightarrow {}^7F_1)$—would be smaller or larger than 1 depending on the concentration and/or the matrix, a phenomenon that could not be explained. Ln^{III} spectra of solid salts and oxides are mainly composed of sharp and weak lines that were ascribed to intraconfigurational f–f transitions in the 1920s by Bethe, Kramer, and Becquerel, but interpreting them necessitated a detailed and novel theory.

3 UNDERSTANDING RARE-EARTH OPTICAL SPECTRA

3.1 Identifying Electronic Levels and Determining Their Energy

Part of the truth was unveiled by Van Vleck who published a seminal paper in 1937: "The puzzle of rare-earth spectra in solids" [29]. At that time electronic structure and chemical bonding theories were at hand, as well as crystal-field theory put forward by Bethe in 1929 [30]. It was also established that the ground-state electronic configuration of Ln^{III} ions was $[Xe]4f^n$ ($n = 0$–14); note that most divalent ions have the same electronic configuration ($n = 0$–5, Ce–Eu; $n = 6$–11, Tb–Yb) with the exceptions of La and Gd ($[Xe]4f^{N-1}5d^1$, $N = 1$ and 8) as well as Lu ($[Xe]4f^{14}6s^1$).[1] Van Vleck addressed two main issues: (i) assignment of the sharp vs broad lines and (ii) why are the faint lines observed at all? Regarding the first point, sharp lines were referred correctly to intraconfigurational f–f transitions, while broad bands in the Ce^{III} and Yb^{III} spectra were assigned to allowed interconfigurational d–f transitions, which is correct for cerium but not for ytterbium for which d-levels lie at energies larger than 70,000 cm^{-1} (<140 nm) [31]; instead they correspond to charge transfer transitions. Concerning f–f transitions, Van Vleck stated that the most intense ones have electric dipole character, while fainter transitions are magnetic dipole transitions. He postulated that formally forbidden electric dipole transitions are observed because of a "distortion of the electronic motion by crystalline fields." He also established that this "distortion" arises only if the ligand field symmetry is devoid of inversion center; otherwise orbital mixing cannot occur. He also evoked the possibility of these transitions having a quadrupolar character and made a rough estimate of the probabilities for quadrupolar, magnetic dipole, and electric dipole transitions. Equally important, Van Vleck realized that interactions between vibrations and electron motion result in additional "vibronic" lines in the spectra and/or in broadening of some lines. In a way, this contribution can be compared to the order brought in the jungle of known elements by the Periodic Table, and it paved the way for Dieke's electronic level diagrams, crystal field analysis, and Judd–Ofelt theory.

The arduous task of finding, calculating, and assigning energy levels in transition metal-containing compounds was subsequently undertaken in the 1940s, particularly by Racah, and enabled quantitative fits of the ligand-field (LF) sublevels for the entire lanthanide series to be performed thanks to the work of B. G. Wybourne [32]. The first synopsis of the $4f^n$ energy levels of all trivalent lanthanides doped in various crystals and spanning the entire ultraviolet (UV),

1. This is valid for ions in gas phase and for inorganic compounds. Recently, W. Evans' group has demonstrated that all divalent Ln ions can be stabilized in organometallic compounds. Magnetic and spectroscopic data show that Nd, Sm, Eu, Dy, Tm, Yb have $4f^n$ configuration, while La, Pr, Gd, Ho, Er, Lu have $4f^{n-1}5d^1$ electronic structure; Ce and Tb are borderline. See Chapter 293 in this volume. "Expanding the +2 Oxidation State to the Rare-Earth Metals, Uranium, and Thorium in Molecular Complexes" by David H. Woen and William J. Evans.

visible, and NIR spectral ranges was given by G. H. Dieke [33]. The $4f^n$ configurations generate many electronic levels, up to 327 for Gd^{III}, characterized by three quantum numbers, S, L, and J, and further split by weak ligand-field effects, on the order of $10^2\ cm^{-1}$, yielding a multitude of LF sublevels, up to 3436 for Gd^{III}. The number of sublevels for the $4f^{n-1}5d^1$ configurations is far larger, culminating at 37,323 for Tb^{III} for instance as shown in Table 1. From the latter, one sees that these two configurations generate almost 200,000 electronic sublevels for the series of 15 elements, which makes understandable the difficulties encountered in identifying them! But on the other hand, these electronic manifolds offer an unlimited playground to spectroscopists and materials scientists for designing tailored luminescent materials.

TABLE 1 Maximum Number of Electronic Levels, Labels of the Ground Level, And Maximum Number of LF Sublevels for $4f^n$ Electronic Configurations of the Trivalent Lanthanide Ions, As Well As Maximum Number of LF Sublevels of the $4f^{n-1}5d^1$ Configurations [26]

		$4f^n$ Configuration			$4f^{n-1}5d^1$ Configuration
Element	*n*	*Number of* SLJ *Levels*	*Ground Level*	*Number of LF Sublevels*	*Number of LF Sublevels*
La	0	1	$^1S_0$	1	–
Ce	1	2	$^2F_{5/2}$	14	10
Pr	2	13	$^3H_4$	91	231
Nd	3	41	$^4I_{9/2}$	364	1274
Pm	4	107	$^5I_4$	1001	4641
Sm	5	198	$^6H_{5/2}$	2002	12,012
Eu	6	295	$^7F_0$	3003	23,023
Gd	7	327	$^8S_{7/2}$	3432	33,462
Tb	8	295	$^7F_6$	3003	37,323
Dy	9	198	$^6H_{15/2}$	2002	32,032
Ho	10	107	$^5I_8$	1001	21,021
Er	11	41	$^4I_{15/2}$	364	10,374
Tm	12	13	$^3H_6$	91	3731
Yb	13	2	$^2F_{7/2}$	14	924
Lu	14	1	$^1S_0$	1	141
Total	—	1641	—	16,384	180,199

In the 1950s and 1960s a vast effort was made first to correctly identify the energy levels of $4f^n$ trivalent ions, both experimentally and theoretically, and, second, to understand the intensity of the f–f transitions through what is now known as the Judd–Ofelt theory. Energy levels were first identified in doped crystals from absorption and emission spectra, resulting in the publication of Dieke's diagrams that were limited to energies of about 40,000 cm^{-1} [33], and then in solution [6]. Both crystal (or ligand) field [34] and Judd–Ofelt [24,35] theories then provided deep understanding on the splitting of the lines and their intensities. Numerous theoretical and experimental studies have then broadened this knowledge, particularly with respect to extending electronic diagrams first to 50,000 cm^{-1} thanks to calculations and experiments conducted at Argonne National Laboratory (USA). Further extension in the vacuum UV up to 70,000 cm^{-1} was made possible by the availability of cyclotron radiation sources [36]. Furthermore, diagrams for divalent and tetravalent ions have also been established, progresses made in theoretical chemistry allowing for precise calculations of these levels (see Chapter 284, Theory of Rare-Earth Electronic Structure and Spectroscopy by Michael Reid, and Chapter 285, Ab Initio Calculations on Excited States of Lanthanide Containing Materials by Luis Seijo and Zoila Barandiaran, in this volume). This is illustrated in Figs. 1–3 for

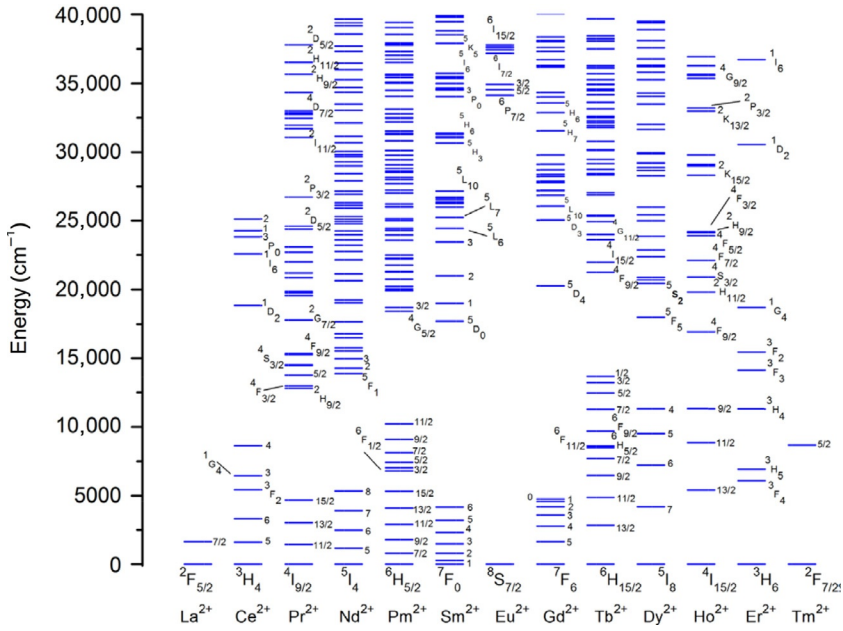

FIG. 1 Calculated energy levels of the divalent lanthanides in the energy range up to 40,000 cm^{-1}. *Reproduced with permission from C.G. Ma, M.G. Brik, D.X. Liu, B. Feng, Y. Tian, A. Suchocki, Energy level schemes of f^N electronic configurations for the di-, tri-, and tetravalent lanthanides and actinides in a free state, J. Lumin. 170 (Pt. 2) (2016) 369–374, © 2016 Elsevier Science B.V.*

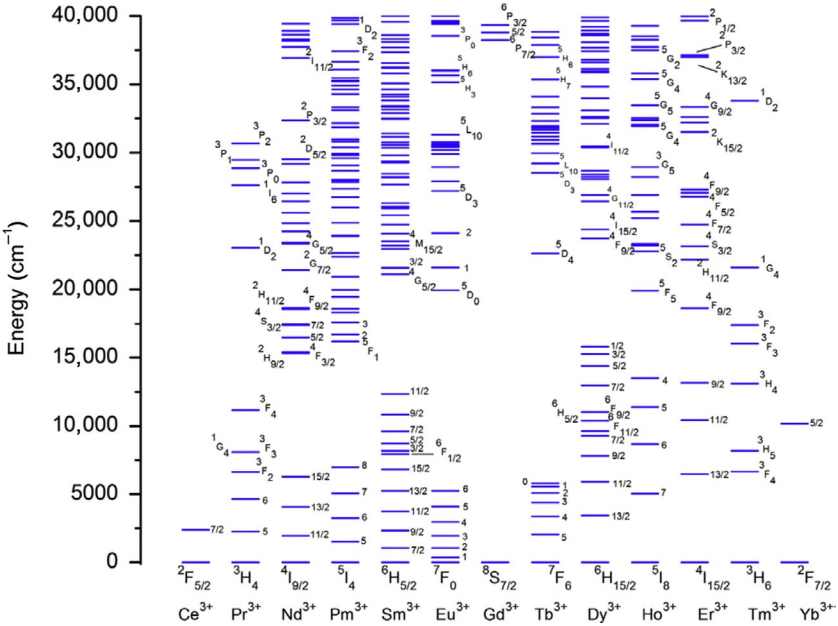

FIG. 2 Calculated energy levels of the trivalent lanthanides in the energy range up to 40,000 cm^{-1}. *Reproduced with permission from C.G. Ma, M.G. Brik, D.X. Liu, B. Feng, Y. Tian, A. Suchocki, Energy level schemes of f^N electronic configurations for the di-, tri-, and tetravalent lanthanides and actinides in a free state, J. Lumin. 170 (Pt. 2) (2016) 369–374, © 2016 Elsevier Science B.V.*

divalent, trivalent, and tetravalent Ln ions, respectively, where levels are plotted up to about 42,500 cm^{-1}. Recent calculations with a fully relativistic first-principles many-electron method performed on $4f^n$ and $4f^{n-1}5d^1$ electronic configurations [26] have allowed further extension of Dieke's diagrams way beyond 100,000 cm^{-1}. Fig. 4 reproduces the levels for $4f^n$ and $4f^{n-1}5d^1$ configurations of the Ln^{III} ions; it clearly points to the lowest levels of the $4f^{n-1}5d^1$ configurations being usually above 50,000 cm^{-1}, making difficult to record the corresponding transition unless vacuum UV instrumentation is at disposal.

3.2 Main Features of Interconfigurational, Intraconfigurational, and Charge-Transfer Transitions in Ln-Containing Luminescent Materials

3.2.1 Laporte's Allowed d↔f Transitions [36,37]

It is to be stressed here that in addition to Laporte's selection rule, the spin rule has to be taken into consideration as well ($\Delta S = 0$) so that only spin-allowed d↔f transitions have sizeable intensity; they are essentially observed for Ce^{III}, Pr^{III}, Tb^{III}, and some Ln^{II} ions (Ln = Sm, Eu, Tm, Yb) since for the other Ln^{III}

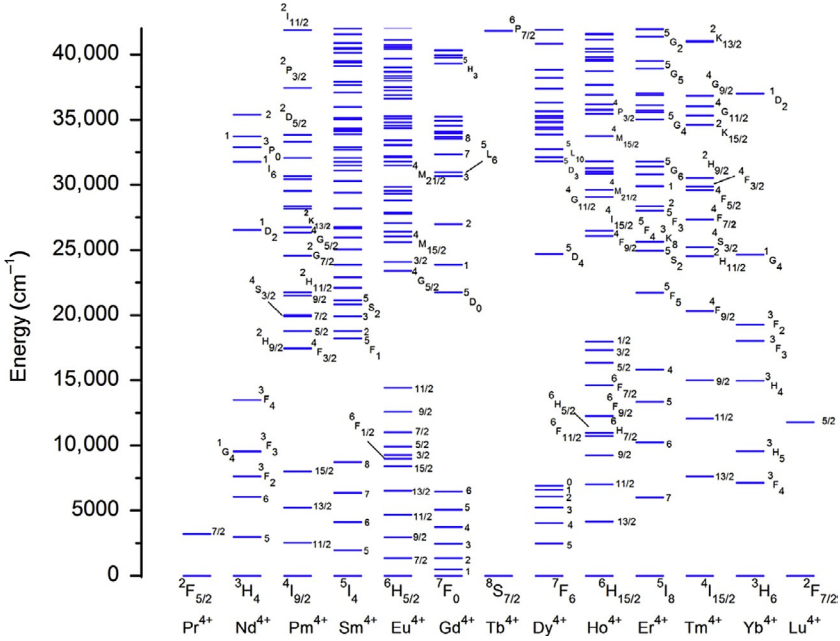

FIG. 3 Calculated energy levels of the tetravalent lanthanides in the energy range up to 42,500 cm^{-1}. *Reproduced with permission from C.G. Ma, M.G. Brik, D.X. Liu, B. Feng, Y. Tian, A. Suchocki, Energy level schemes of f^N electronic configurations for the di-, tri-, and tetravalent lanthanides and actinides in a free state, J. Lumin. 170 (Pt. 2) (2016) 369–374, © 2016 Elsevier Science B.V.*

ions these transitions are often quenched by intersystem crossing to the 4f^n configuration. Spin-forbidden transitions are still observed, but their identification is made difficult in view of their smaller intensity. The d↔f transitions occur at high energy, usually >50,000 cm^{-1} (<200 nm) [31]. They have been documented both theoretically (e.g., calculations in the gas phase by Brewer [38]) and experimentally in several hosts, such as CaF_2, $LiYF_4$, or $Y_3Al_5O_{12}$ (YAG) [39,40]. As an example, energies of the first spin-allowed f→d transition of Ln^{III} ions doped in calcium fluoride are reported in Fig. 5 (top); they correspond to excitation into the ^{2}E levels. For Tb^{III}, this transition occurs at 216 nm (0-phonon component), but less intense bands are seen at longer wavelengths that correspond to spin-forbidden transitions (Fig. 5, bottom). In this figure, HS_1 is the 0-phonon line, while HS_1' is the first vibronic component (475 cm^{-1} assigned to the breathing mode of the fluorides around Tb^{III}). When d-orbitals are implied, the ligand field generated by the surrounding ligands is much larger (10^3–10^4 cm^{-1}) than for f-orbitals. This is exemplified in the energy separation between the low- and high-spin fd states amounting to ≈7900 cm^{-1} [39]. Another consequence of the external nature of d-orbitals lies

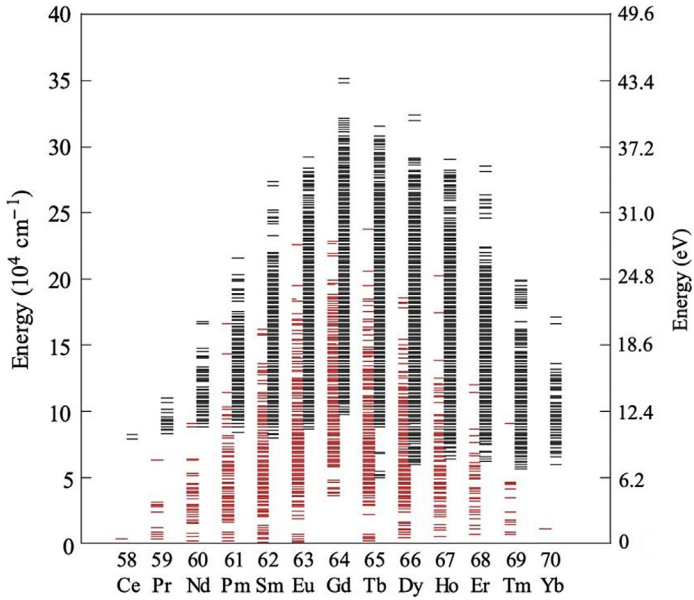

FIG. 4 Complete $4f^n$ (*left*, *red*) and $4f^{n-1}5d^1$ (*right*, *black*) energy diagram for all trivalent Ln ions as calculated by the fully relativistic first-principles many-electron method. Note the *right scale* in eV (1 eV corresponds to 8066 cm^{-1}). *Reproduced with permission from K. Ogasawara, S. Watanabe, H. Toyoshima, M.G. Brik, First-principles calculations of 4f-4f5d transition spectra, in: K.A. Gschneidner Jr., J.-C.G. Bünzli, V.K. Pecharsky (Eds.), Handbook on the Physics and Chemistry of Rare Earths, vol. 37, Elsevier Science B.V., Amsterdam, 2007, pp. 1–59 (Chapter 231), © 2007 Elsevier Science B.V.*

in Stokes shifts being much larger than for f-states, typically between 1000 and 3000 cm^{-1}, as well as in the easy tunability of the energy of d↔f transitions by modifying the nature of the inner coordination sphere of the emitting ions (e.g., by doping in different matrices). A stronger ligand field will induce larger splitting with, as a consequence, the lowest fd state being pushed toward lower energy and the emission wavelength sustaining a red shift.

Owing to their importance for the phosphors used in lighting and displays, d↔f transitions have been thoroughly and systematically studied. The actual position of the lowest fd state with respect to valence and conduction bands is important in this respect since it determines the luminescent properties of the activators (excitation and emission wavelengths, multiphonon relaxation, trapping, and detrapping of charge carriers). A phenomenological equation has been proposed by Dorenbos for estimating its energy with respect to that of Ce^{III}:

$$E(\mathrm{Ln}, A) = 49{,}340\,\mathrm{cm}^{-1} - D(A) + \Delta E^{\mathrm{Ln,Ce}} \tag{1}$$

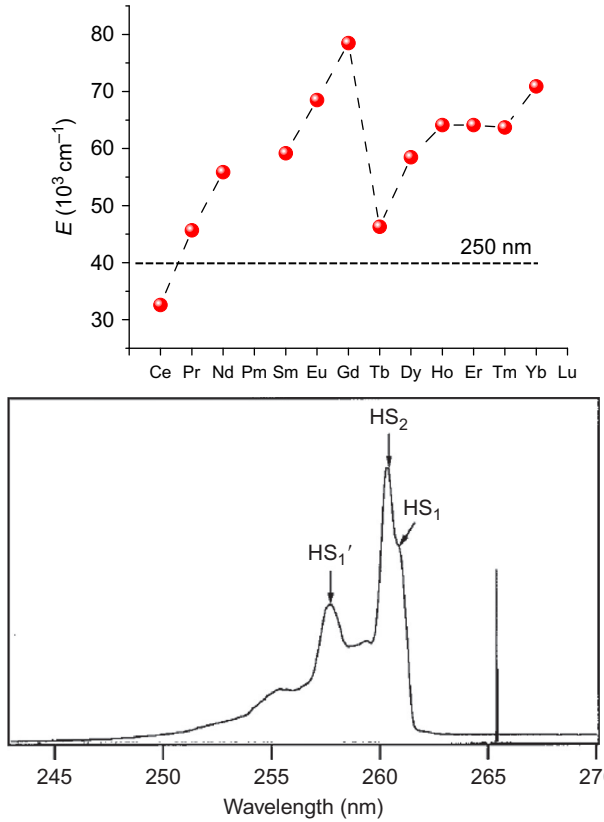

FIG. 5 (*Top*) Energies of the first spin-allowed f→d transitions of Ln^{III} ions doped in CaF_2. (*Bottom*) Excitation spectrum for a CaF_2 crystal doped with 0.1% Tb^{III} recorded monitoring the $^5D_4 \rightarrow {}^7F_5$ transition at 544 nm at 6 K and showing the energy region in which the spin-forbidden transition to the high-spin fd state is observed; the *dotted line* below is the calculated spectrum. Top panel*: Redrawn from P. Dorenbos, f -> d transition energies of divalent lanthanides in inorganic compounds, J. Phys. Condens. Matter 15 (2003) 575–594*. Bottom panel*: Reproduced with permission from L. van Pieterson, M.F. Reid, G.W. Burdick, A. Meijerink, 4f(n)-> 4f(n-1)5d transitions of the heavy lanthanides: experiment and theory, Phys. Rev. B 65 (2002) Art. Nr. 045114, © 2002 The American Physical Society.*

where $E(\mathrm{Ln}, A)$ is the maximum of the lowest f→d band of a Ln^{III} ion lying on a given site of host lattice A. The contribution $D(A)$ is the lowering of the energy of the fd state of Ce^{III} by LF effects (with respect to the free ion value). Finally, $\Delta E^{\mathrm{Ln,Ce}}$ is the energy difference between the lowest df states of a Ln^{III} ion and Ce^{III}, which is host independent. These two parameters are known from the analysis of a large number of materials [41]. More recently, Zych *et al*. proposed to use the energy of the zero-phonon line rather than the peak maximum to more accurately estimate the energies of the df states [42].

3.2.2 Intraconfigurational f–f Transitions [1,43,44]

A transition between two electronic states is achieved thanks to an "operator." Given the nature of light, three main operators may be effective, electric dipoles (EDs), magnetic dipoles (MDs), and electric quadrupoles (EQs). Laporte's parity selection rule implies that states with the same parity cannot be connected by electric dipole transitions; as a consequence, f–f transitions are forbidden by the ED mechanism. However, when lanthanide ions are under the influence of a ligand field, noncentrosymmetric interactions allow the mixing of electronic states of opposite parity into the 4f wavefunctions, which relaxes the selection rules and the transitions become partially allowed; they are called *induced* (or forced) *electric dipole transitions*. Magnetic dipole transitions are allowed, but their intensity is weak; in 4f–4f spectra however they frequently have intensity of the same order of magnitude as induced electric dipole transitions. Quadrupolar transitions are also parity allowed, but they are much weaker than MD transitions so that they are usually not observed or identified. Some induced ED transitions are highly sensitive to minute changes in the Ln^{III} environment and are called *hypersensitive* or sometimes *pseudo-quadrupolar transitions* because they apparently follow the selection rules of EQ transitions.

There are selection rules for each quantum number (ℓ, S, L, J), as well as symmetry-related selection rules. Rules applying to S, L, and J quantum numbers are given in Table 2; for symmetry-related selection rules, please refer to Refs. [34,46].

In 1962, two researchers, B. R. Judd and G.S. Ofelt submitted independently within a month a paper dealing with the same subject: intensities of

TABLE 2 Selection Rules on *S*, *L*, *J* Quantum Numbers for f–d and f–f Transitions [45]

Transition	ΔS	$\lvert\Delta L\rvert$[a]	$\lvert\Delta J\rvert$[b]	Approx. Oscill. Strength[c]
ED (d–f)	0	≤1	≤1	0.01–1
Forced ED (f–f)	0	≤6 (2, 4, 6 if L or $L'=0$)	≤6 (2, 4, 6 if J or $J'=0$)	10^{-4}–10^{-5}
Vibronic (ED, f–f)	Same as forced ED			10^{-7}–10^{-10}
MD (f–f)	0	0	0, ±1	10^{-5}–10^{-6}
EQ (f–f)	0	0, ±1, ±2	0, ±1, ±2	10^{-10}

[a] $L=0 \leftrightarrow L'=0$ *transitions are always forbidden.*
[b] $J=0 \leftrightarrow J'=0$ *transitions are always forbidden.*
[c] *Spin-allowed transitions; spin-forbidden transitions are about 100 times less intense.*

f–f transitions. Now known as Judd–Ofelt (JO) theory, the corresponding model has been established within the frame of the crystal field concept and it provides a simple scheme for reproducing the intensities of f–f absorption spectra. One drawback is that it only takes into account the $4f^n$ electronic configuration, that is, interconfigurational $4f^n$–$4f^{n-1}5d^1$ interactions are neglected. On the other hand, spin-orbit coupling is treated within the frame of the intermediate coupling scheme. The dipole strength in $esu^2\,cm^2$ ($=10^{36}\,D^2$) of an induced ED f–f transition between states ψ and ψ' is given by:

$$D_{\mathrm{ED}} = e^2 \cdot \sum_{\lambda=2,4,6} \Omega_\lambda \cdot \left|\left\langle \Psi \middle\| U^\lambda \middle\| \Psi' \right\rangle\right|^2 \tag{2}$$

in which e is the electric charge of the electron, wavefunctions ψ and ψ' are full intermediate-coupled functions $f^n[SL]J$, U^λ are the irreducible tensor forms of the ED operator, and Ω_λ are the phenomenological Judd–Ofelt parameters, expressed in cm^2. The bracketed expressions in Eq. (2) are dimensionless doubly reduced matrix elements which are insensitive to the metal-ion environment.

JO parameters are adjustable parameters and they are calculated from the absorption spectrum $\varepsilon(\tilde{\nu})$. For an isotropic crystal or a solution, the experimental dipole strength is defined as:

$$D(\exp) = \frac{10^{-36}}{108.9 \cdot \tilde{\nu}_{\mathrm{mean}} \cdot X_{\mathrm{A}}} \cdot \left((2J+1) \cdot \frac{9n}{(n^2+2)^2} \right) \cdot \int \varepsilon(\tilde{\nu}) \mathrm{d}\tilde{\nu} \tag{3}$$

with X_{A} being the fractional population of the initial state while $\tilde{\nu}_{\mathrm{mean}}$ is given by:

$$\tilde{\nu}_{\mathrm{mean}} = \frac{\int \tilde{\nu} \cdot \varepsilon(\tilde{\nu}) \mathrm{d}\tilde{\nu}}{\int \varepsilon(\tilde{\nu}) \mathrm{d}\tilde{\nu}} \tag{4}$$

Finally, $(2J+1)$ is the degeneracy of the initial state and the expression involving the refractive index n is known as Lorentz's local field correction. Calculations of transition probabilities within the frame of JO theory are usually made assuming that all LF sublevels within the ground level are equally populated and that the material under investigation is optically isotropic. The former hypothesis is only reasonable in some cases, e.g., when transitions initiate from nondegenerate states such as $Eu(^7F_0)$. The second assumption is not valid for uniaxial or biaxial crystals, but, of course, holds for solutions.

The phenomenological JO parameters are determined from a fit of Eq. (2) to the experimental values defined by Eq. (3), using adequate matrix elements. The exact procedure is described in details in Refs. [24,35]. In the case of Eu^{III} the procedure is simpler since Ω_2, Ω_4, and Ω_6 can be directly extracted from the dipole strength of the $^5D_2 \leftarrow {}^7F_0$, $^5D_4 \leftarrow {}^7F_0$, and $^5L_6 \leftarrow {}^7F_0$ transitions,

respectively. Extensive tabulations of JO parameters can be found in Ref. [24], while spectra for all Ln^{III} ions are presented in Ref. [6].

The rearrangement consecutive to the promotion of an electron into a 4f orbital of higher energy does not perturb much the binding pattern in the molecules since 4f orbitals do not participate substantially in this binding. As a consequence, the internuclear distances remain almost the same in the excited state, which generates narrow bands and very small Stokes shifts, at least when the Ln ion is excited directly into the f–f transition. Large ligand-induced Stokes shifts are generated when excitation goes through coordinated ligands and/or the matrix into which the emitting ion is imbedded. Selection rules for emission are the same as for absorption. The emission probability is given by Einstein's rates of spontaneous emission A from an initial state $|\Psi_J\rangle$, characterized by a quantum number J, to a final state $|\Psi'_{J'}\rangle$:

$$A\left(\Psi_J, \Psi'_{J'}\right) = k^{\text{rad}} = \frac{1}{\tau^{\text{rad}}} = \frac{64\pi^4\widetilde{\nu}^3}{3h(2J+1)}\left[\frac{n(n^2+2)^2}{9}D_{\text{ED}} + n^3 D_{\text{MD}}\right] \tag{5}$$

where $\widetilde{\nu}$ is the mean energy of the transition defined in Eq. (4), h is Planck's constant, n is the refractive index; D_{ED} is given by Eq. (3) and D_{MD} by Eq. (6):

$$D_{\text{MD}} = \left(\frac{e \cdot h}{4 \cdot \pi \cdot m_e \cdot c}\right)^2 \cdot \left|\langle \Psi || L + 2S || \Psi' \rangle\right|^2 \tag{6}$$

The bracketed matrix elements are tabulated and the radiative lifetime can therefore be extracted from the spectral intensity, that is, from Eqs. (2), (5), and (6). Except in few cases, this calculation is not trivial and large errors may occur, including those pertaining to the hypotheses made within Judd–Ofelt theory.

If the absorption spectrum corresponding to an emission spectrum is known, which may be the case when the luminescence transitions terminate onto the ground level, the radiative lifetime can be simply calculated from the following equation where N_A is the Avogadro's number (6.023×10^{23}):

$$\frac{1}{\tau^{\text{rad}}} = 2303 \times \frac{8\pi c n^2 \widetilde{\nu}^2 (2J+1)}{N_A(2J'+1)} \int \varepsilon(\widetilde{\nu}) \mathrm{d}\widetilde{\nu} \tag{7}$$

In the special case of Eu^{III} for which one transition ($^5D_0 \rightarrow {}^7F_1$) has pure magnetic origin, a convenient simplified equation can be derived [47]:

$$A\left(\Psi_J, \Psi'_{J'}\right) = \frac{1}{\tau^{\text{rad}}} = A_{\text{MD},0} \cdot n^3 \left(\frac{I_{\text{tot}}}{I_{\text{MD}}}\right) \tag{8}$$

It is to be stressed that the radiative lifetime depends on the refractive index, on the chemical environment of the emitting ion (bond polarizability), and on the specific emitting level.

3.2.3 Charge Transfer Transitions

Charge transfer transitions play an ambiguous role with respect to lanthanide luminescence. They are essential in sensitizing the luminescence of lanthanide-containing inorganic phosphors, but they can be totally detrimental in other instances, quenching light emission completely. As for d↔f transitions, they are parity allowed and therefore intense. Three main types of charge transfer transitions may be present:

- Ligand-to-metal charge transfer (LMCT) states. During the process, an electron is transferred from the surrounding to the metal ion. As for the 4f–5d transitions, their energies are large so that corresponding transitions are often observed in the UV spectral range. The lowest energies occur for the easily reducible ions, namely, Sm^{III}, Eu^{III}, Tm^{III}, and Yb^{III} as shown in Fig. 6 which displays calculated $2p(O) \rightarrow Ln$ transitions for inorganic phosphors. The LMCT energies, however, depend heavily on the host materials and for Eu^{III}, a transition as low in energy as 31,250 cm^{-1} has been reported for europium azide in water [48]. Covalent contribution to the bonding by organic ligands considerably lowers the energy of the LMCT state in the range 18–25,000 cm^{-1}, and the energy can be modulated by substitution at the coordinating ligands [49]. Mixing of LMCT and 4f states leads to enhanced forced electric dipole transitions. As an example, the very weak $Eu(^5D_0 \leftarrow {}^7F_0)$ absorption with $\varepsilon = 10^{-3}$ M^{-1}-cm^{-1} for the aqua ion $[Eu(H_2O)_9]^{3+}$ at 17,212 cm^{-1} is not only blue shifted to 17,330 cm^{-1} in the binuclear complex with *p*-Bu^t-calix[8]arene H_8L, $[Eu_2(H_2L)(DMF)_5]$, but its absorptivity is enhanced by a factor 5000,

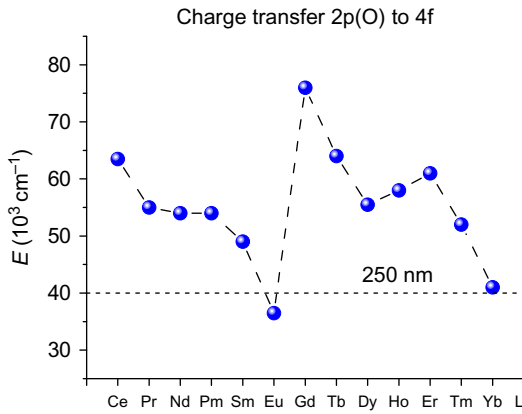

FIG. 6 Calculated energies of the O(2p)-to-Ln^{III} charge transfer states. *Redrawn from T. Kano, Principal phosphor materials and their optical properties: luminescence centers of rare-earth ions, in: S. Shionoya, W.M. Yen (Eds.), Phosphor Handbook, CRC Press Inc., Boca Raton, FL, 1999, pp. 177–200.*

to reach $\varepsilon = 5\ M^{-1}\ cm^{-1}$ [50,51]! This phenomenon is called intensity stealing.

- Metal-to-ligand charge transfer (MLCT) states. These states are commonly observed with d-transition metal ions, but are rarely identified in spectra of lanthanide complexes, except for Ce^{III}, which is easily oxidized into Ce^{IV}.
- Ligand-centered charge transfer states. If the ligand has polarized domains (e.g., push-pull ligand), then charge transfer can occur between them. The states are referred to as intraligand CTs (ILCTs) or intramolecular CTs (ICTs); sometimes more precision is added to point to the origin of the polarization, such as twisted intraligand CT (TICT). Such states are ideal for sensitizing lanthanide luminescence in view of their large absorptivity and, often, of their relatively low energy; moreover the latter can be modulated by modifying substituents decorating organic ligands [52].

In some heterometallic *n*d–4f polynuclear molecular edifices, singlet or triplet MLCTs, LMCTs, or MMCT (metal-to-metal CT) states linked to the d-transition metal moiety may also act as convenient donors for transferring energy on the Ln excited states [53,54].

4 LUMINESCENCE SENSITIZATION AND ITS MODELING

In 1942, S. I. Weissman discovered that lanthanide luminescence could be generated in molecular complexes by excitation into ligand absorption bands [55]. This observation, called *luminescence sensitization* or *antenna effect*, had a major impact on the development of lanthanide-containing luminescent molecules and materials. The brightness of an emissive compound is indeed related to the product of its molar absorption coefficient by the quantum yield:

$$B = \varepsilon(\lambda_{exc}) \times Q \tag{9}$$

The antenna effect allows one to boost the low brightness of Ln ions ($<5\ M^{-1}\ cm^{-1}$) to values up to 10^5–$10^6\ M^{-1}\ cm^{-1}$.

4.1 Energy Transfer Mechanisms

The next point was to unravel the nature of the energy transfer. In 1953, D. L. Dexter extended Th. Förster's dipole–dipole mechanism for energy transfer between fluorescent molecules [56] to forbidden transitions in luminescent solids [57]. He identified several potential mechanisms for energy transfer, each having different distance dependence (Table 3). To get a rough idea of the relative importance of these mechanisms he calculated the number of activator sites that can be excited by a single sensitizer; this estimate is based on a solid having NaCl structure and corresponding site separations. Interestingly, one sees that the electric dipole–quadrupole mechanism is of comparable importance with the exchange mechanism. In activator-doped solids,

TABLE 3 Energy Transfer Mechanisms Between Sensitizer and Activator and Their Distance Dependence

Mechanism	Distance Dependence	Nr Excited Sites
Dipole–dipole (electric)	r_{da}^{-6}	10^3–10^4
Dipole–quadrupole (electric)	r_{da}^{-8}	10^2
Exchange (spin)	$e^{-r_{da}}$	30–40
Quadrupole–quadrupole (electric)	r_{da}^{-10}	n.a.
Electric dipole–magnetic dipole	n.a.	Negligible

experimental distinction between dipole (d) and quadrupole (q) mechanisms can be done by plotting the luminescence intensity of the sensitizer vs the concentration of the activator:

$$\frac{I_0^S}{I^S} \propto c_A^{\alpha/3} \tag{10}$$

with $\alpha = 6$, 8, and 10 for d–d, d–q, and q–q mechanisms, respectively.

This is illustrated in Fig. 7 for the phosphor $NaCaY(PO_4)_2:Eu^{II}(1\%)$, $Mn^{II}(x\%)$ in which Eu^{II} sensitizes the luminescence of divalent manganese. The plot with $\alpha = 6$ is clearly nonlinear, contrary to the plot with $\alpha = 8$, pointing to a major contribution from the dipole–quadrupole mechanism [58].

4.2 Influence of Various Electronic States

The energy transfer process is highly complex. In addition to the various mechanisms that can operate, several energy states may be implied both from the donor and the acceptor. A detailed discussion is out of the scope of this essay so that potential donor states are simply listed below for the case of coordination complexes. For a more detailed discussion, please refer to Ref. [44].

- *Triplet states*. Since these states have long lifetimes, energy transfer can effectively compete with phosphorescence so that they are often invoked as being the main donor states. Therefore, several experimental relationships have been proposed between quantum yields and the energy difference between the 0-phonon component of the triplet state and the emitting level. For Eu^{III} and Tb^{III}, ideal energy gaps are between 2000 and 4000 cm^{-1}. However, this approach is far too simplistic in that it only concentrates on energy transfer, whereas the quantum yield is also affected

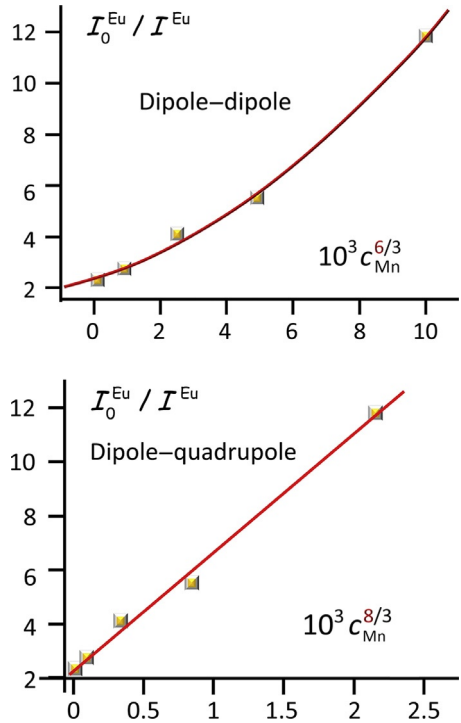

FIG. 7 Plots of emission intensity of the sensitizer (Eu^{II}) vs concentration of the activator (Mn^{II}) in $NaCa(PO_4)_2$:Eu^{II}(1%)Mn^{II}(x%) (x = 1, 3, 5, 7, 10) according to Eq. (10): (*top*) $\alpha = 6$, (*bottom*) $\alpha = 8$. *Redrawn from W.R. Liu, P.C. Lin, A study on luminescence properties and energy transfer mechanism for NaCaY(PO4)2:Eu2+,Mn2+ phosphors for LED applications, Opt. Express 22 (2014) A446–A451.*

by nonradiative deactivation in the coordination sphere (e.g., water coordination). Moreover, the accepting state of the Ln ion is not necessarily the emitting state. Finally, charge transfer states may considerably perturb this simple scheme.

- *Singlet states*. Observation of Ln luminescence upon ligand excitation in some lanthanide chelates despite that the energy of the triplet state was lower than the Ln emitting state prompted M. Kleinerman in 1969 to invoke energy transfer from the singlet state: "Contrary to prevailing notions, it is shown [in this paper] that energy transfer does not require the participation of the lowest triplet level of the chelate" [59]. More recently several examples of singlet-state sensitization have been reported, some involving in fact ^{1}ILCT or ^{1}MLCT states.
- *Charge transfer states*. As mentioned above they may interfere with the energy transfer mechanism, in a positive or negative way. Sometimes they act as simple relays in the energy transfer process [60].

- *Weak interaction*s. These interactions may generate new aggregated species with different electronic levels than the parent moieties. They cannot be neglected, and presently studies on aggregation-induced luminescence are gaining momentum. It is noteworthy that similarly to CT states, aggregation can also trigger emission quenching [61].

In fact, the sensitization process is described by a complex kinetic scheme with numerous rate constants (for each transfer, back transfer has also to be considered). A dominant pathway will emerge only if the corresponding rate constants are the largest. In order to discuss energy transfer in a correct way, the following parameters should be determined: (i) the overall (or external) quantum yield determined upon ligand excitation, Q_{Ln}^{L}; (ii) the intrinsic (or internal) quantum yield measured upon f–f excitation, Q_{Ln}^{Ln}; (iii) the lifetime of the emitting state, τ_{obs}; (iv) the radiative lifetime, τ_{rad}; and (v) the sensitization efficiency, η_{sens}. These parameters are linked by the following equation:

$$\eta_{sens} = \frac{Q_{Ln}^{L}}{Q_{Ln}^{Ln}} = Q_{Ln}^{L} \times \frac{\tau_{rad}}{\tau_{obs}} \tag{11}$$

If Q_{Ln}^{Ln} cannot be determined experimentally, it can be estimated if the lifetimes are known. The radiative lifetime can be calculated from the set of equations (2), (5), and (6) or from Eq. (7) or, for Eu^{III}, from Eq. (8). The only other needed parameter is the refractive index n that can easily be measured. Note that Q_{Ln}^{Ln} reflects the effect of nonradiative deactivations in the Ln surroundings and that it is always larger than, or at most equal to, Q_{Ln}^{L}.

4.3 Modeling the Energy Transfer Process

Theoretical modeling of the energy transfer processes in Ln^{III} complexes with organic ligands has been initially proposed by G. F. de Sá *et al.* [62]. In a first step, the geometry of the complex is optimized within the frame of a semiempirical molecular orbital model; the bonding in lanthanide complexes having essentially an ionic character is simulated with a central potential model, known as the sparkle model. Proper parameterization with Gaussian functions has been achieved by initially reproducing the known structure of several Eu^{III} complexes [62,63], but has been rapidly extended to other lanthanide ions and, presently, parameters are available for the entire series, from La^{III} to Lu^{III} [64].

Energies and transition moments of the ligand excited states are then calculated with the intermediate neglect of differential overlap/single-configuration interaction (INDO/S-CI) method. Despite the purely ionic model used, calculated and experimental electronic spectra are in usually in fairly good agreement. More sophisticated methods for calculating triplet state energies, for instance, ab initio complete active space self-consistent field or time-dependent density functional calculations (TD-DFTs), are also commonly used.

Finally, the quantum yield is calculated taking into account a kinetic model including differential expressions for the transfer rates. The transfer rates, W_{ET}, are expressed within the Fermi theory which assumes the validity of Born–Oppenheimer approximation. The kinetic model simply expresses the population variation of the levels implied within the steady-state approximation:

$$\frac{\partial p_i}{\partial t} = -\sum_{j \neq i} k_{ij} p_i + \sum_{j \neq i} k_{ji} p_j = 0 \tag{12}$$

The system of equations is solved by Runge–Kutta method with adaptive integration steps and the theoretically estimated quantum yield is given by:

$$Q = \frac{A_{tot} \cdot p_j}{\Theta \cdot p_i} \tag{13}$$

here A_{tot} refers to the sum of the radiative and nonradiative rates ($=1/\tau_{obs}$) and Θ is the pumping rate in photons/s. The model requires estimates of some parameters, such as nonradiative decay rates for internal conversion in the Ln^{III} manifolds or the lifetime of the donor state(s) at the temperature at which the transfer occurs, but it nevertheless yields reasonably good results, usually within ±20%. The model has subsequently been improved and the group of R. Freire has produced an open-access computer program for the entire procedure [64].

An example of such a modeling is shown in Fig. 8 for a dimeric Eu^{III} tetrakis(β-diketonate). Little transfer from the singlet state occurs since the

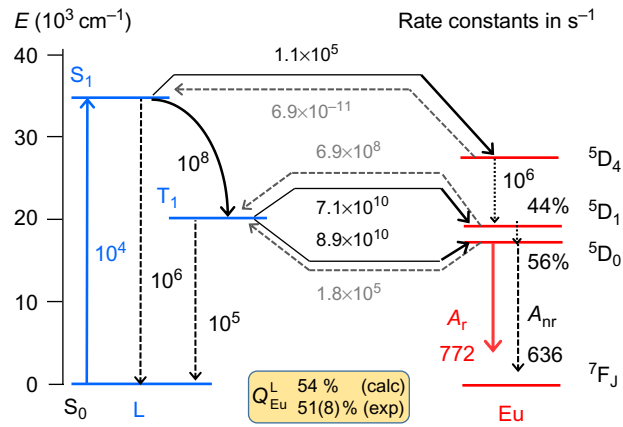

FIG. 8 Calculated rates of transfer and back transfer for a dimeric Eu^{III} tetrakis(β-diketonate). *Adapted from S. Biju, R.O. Freire, Y.K. Eom, R. Scopelliti, J.-C.G. Bünzli, H.K. Kim, A Eu(III) tetrakis(β-diketonate) dimeric complex: photophysical properties, structural elucidation by sparkle/AM1 calculations, and doping into PMMA films and nanowires, Inorg. Chem. 53 (2014) 8407–8417.*

rate constant is one order of magnitude smaller than the fluorescence rate constant and three orders of magnitude smaller than the intersystem crossing rate constant. The rate constants for transfer from the triplet state are very large, and both Eu($^5D_1$) and Eu($^5D_0$) are populated about equally. The calculated quantum yield agrees very well with the experimental one [65].

5 A FIREWORK OF APPLICATIONS

Lanthanide photonics is a burgeoning field because all trivalent lanthanide ions, baring lanthanum and lutetium, behave as ideal wavelength-converting devices with narrow emission bands covering the entire spectral range from UV (Gd) to visible and near-infrared (up to 3 μm). Lifetimes of the excited states tend to be long (ms for phosphorescence, μs for fluorescence) so that luminescence can easily be detected in time-gated mode. In addition, trivalent cerium and some divalent ions, like europium, display broad but widely tunable d–f emission. Selected emission spectra of trivalent lanthanides are shown in Fig. 9, and some applications of lanthanide photonics are briefly outlined below.

5.1 Lasers

Lanthanide ions are ideally suited as active materials for solid-state lasers emitting in the UV, visible, or NIR. One of the most widely used lasers is YAG:Nd^{III} with its mythic line at 1.06 μm, the frequency of which can easily be doubled (532 nm, green; e.g., laser pointers), tripled (355 nm, blue), or quadrupled (266 nm, UV), leading to multi-line lasers for excitation of luminescence spectra. To enhance the yield of YAG:Nd lasers, Cr^{III} or Ce^{III} are often introduced in the garnet as sensitizers. The YAG garnet can be doped

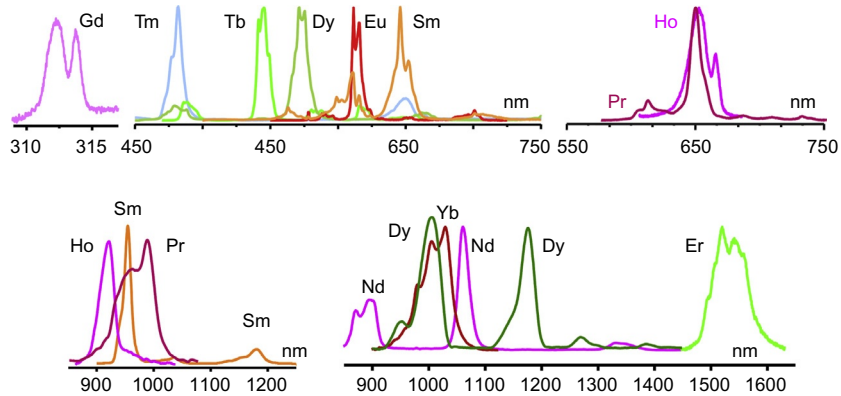

FIG. 9 Emission spectra of selected trivalent lanthanide ions. *Vertical scales* are not comparable.

by several other lanthanide ions, giving rise to devices emitting at 1.03 μm (Yb), 1.93–2.04 μm (Tm), 2.1 μm (Ho, Tm), and 2.94 μm (Er).

Low-power lasers, particularly those emitting at long wavelengths, are central to several medical applications, eye surgery, skin treatment, and dentistry or for monitoring the sugar content in blood. NIR-emitting lasers are one of the major components in telecommunication systems. High-power YAG:Nd lasers are used in manufacturing, while arrays of ultra-high-power Nd-doped phosphate glass lasers provide up to 500 TW power in nuclear fusion experimental facilities in Japan and in the United States.

5.2 Telecommunications

Telecommunications and Internet-providing systems often rely on silica optical fibers, but despite their excellent transparency the signals get attenuated after 50 or 100 km and need amplification. The latter is achieved by erbium-doped fiber amplifiers (EDFAs) that were proposed in 1987. Er^{III} is indeed emitting in the main telecommunication window (C band, 1.5 μm); therefore, silica glasses doped with this ion behave as ideal waveguide amplifiers [66]. The present network of submarine optical fibers is sketched in Fig. 10.

In EDFAs, erbium is excited either at 980 nm, on the $^4I_{11/2}$ level, or at 1480 nm, on a metastable ligand field sublevel of $^4I_{13/2}$. This results in a two-level laser emitting in the range 1530–1550 nm depending on the fine-tuning of the materials into which it is doped. The 980-nm band has higher

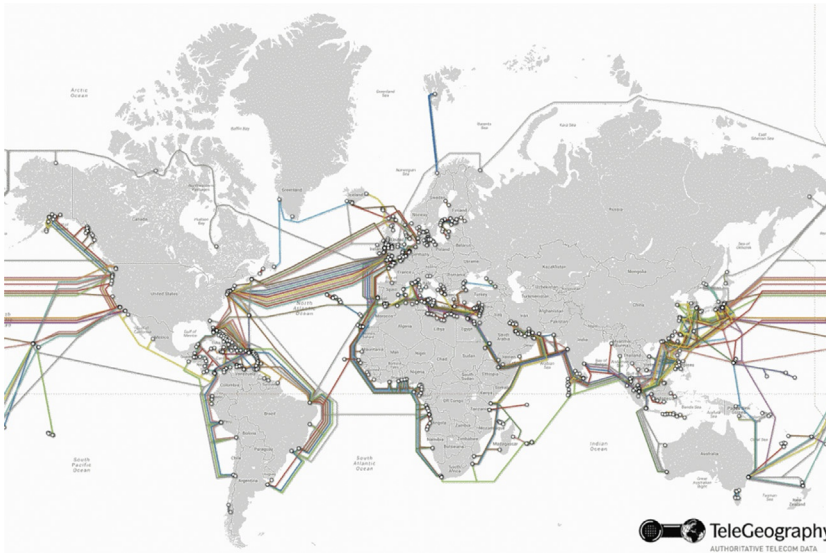

FIG. 10 Submarine cable map 2016. *TeleGeography, http:/www.submarinecablemap.com/ free resource, accessed Aug. 23, 2016.*

absorption cross section, so it is generally used when low-noise performances are required; the transition is narrow and therefore wavelength-stabilized laser sources are needed. The 1480-nm band features a lower absorption cross section but is broader, which makes it ideal for high-power amplifiers. Many EDFAs use a combination of both pump wavelengths.

One of the challenges faced by these systems is the competition with wireless networks. Indeed, the low absorption cross section of Er^{III} f–f transitions and concentration quenching when there are more than 10^{20} Er^{III} ions per cm^{-3} limit the performances of EDFAs. There are several solutions to this problem. The first one is co-doping sensitizers to compensate for the low absorbance of Er^{III} at 980 and 1480 nm; Yb^{III} is particularly adequate for 980-nm pumping since its absorption cross section at that wavelength is about 10 times larger. Moreover, the Yb($^2F_{5/2}$)-excited level efficiently transfers energy onto the resonant Er($^4I_{11/2}$) level that decays faster to the $^4I_{13/2}$ level than back transfer to Yb^{III}. A second solution consists in using hosts different from silica and co-doping high-refractive index components. A third way out is to dope Er^{III} into polymer fibers, for instance, polymethylmethacrylate, with the help of organic fluorinated ligands [3]. The resulting amplifiers have definite technical advantages over silica: better flexibility and larger diameter, allowing optimum coupling to local-scale devices, as well as a much lower pump threshold, up to 660-fold smaller. Presently, much emphasis is put on developing integrated optical devices combining both EDWAs (erbium-doped waveguide amplifiers) and EDWLs (erbium-doped waveguide lasers) on a small 1-mm^2 chip. Optimization of all parameters has led to amplifiers in which the fiber length can be reduced to a few cm thanks to gains up to 935 dB cm^{-1}.

5.3 Lighting

Despite a sharp increase in the number of lighting devices worldwide, the share of electricity devoted to it is continuously decreasing, representing presently only about 12–20% of all electricity used, depending on countries. What is really striking is the prominent role played by rare earths in improving the efficiency of lighting devices (Fig. 11). The historic electric bulb with a very poor efficiency was partly replaced in the 1970s with fluorescent tubes and lamps coated with lanthanide-containing phosphors. The coating was a carefully designed mixture of three phosphors, typically Y_2O_3:Eu^{III} (red emitter), $LaPO_4$:Ce^{III},Tb^{III} (green emitter, Ce^{III} acts as sensitizer), and $BaMgAl_{10}O_{17}$:Eu^{II} (blue emitter). Power efficiency of the luminaires was raised by a factor of 4 compared to incandescent lamps, and the same technology was later introduced in compact fluorescent lamps. These devices contain a small amount of mercury, producing the 254-nm excitation wavelength; when not properly disposed of these lamps cause environmental problems, a reason why their sale is being increasingly banned.

The situation changed in the mid-1990s with the advent of commercial white light-emitting diodes (WLEDs), following the development of GaN

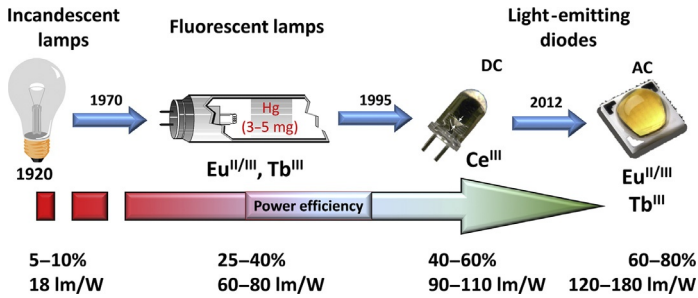

FIG. 11 Impact of rare earths on lighting. Efficiencies are "typical" values, i.e., average of several sources (technology is progressing and numbers keep improving!); luminous efficiency (lm/W) refers to an input electric power of 100 W.

blue LEDs; these devices are much smaller, do not require mercury, and have better lifetime and better efficiency. In the initial design white light was generated by combining the blue emission from (In,Ga)N with the yellow d–f luminescence from $Y_{3-x}Ce_xAl_5O_{12}$ ($0.001 < x < 0.03$, YAG:Ce^{III}, quantum yield >90%), a phosphor that was proposed in 1967 for cathode ray tubes [67]. Initial shortcomings, such as poor color rendering index and high correlated temperature, have since been cured, for instance, by increasing Ce^{III} concentration, co-doping other Ln^{III} ions, or introducing red-emitting Eu^{II} phosphors ($Sr_2Si_5N_8$:Eu^{II}, $CaSiAlN_3$:Eu^{II}).

Following this success, numerous other designs have been investigated, including three-component (RGB) phosphors (e.g., GaN:Ln, Ln = Eu—red, Er—green, and Tm—blue) and careful nanopatterning of the phosphor structure, with the imperative goal of improving brightness. Presently, laboratory luminaires incorporating WLEDs reach brightness in the range 200–250 lm/W. This is a necessity if the general objective of 30% reduction in lighting electricity consumption looked for by most states and international institutions is to be met by 2030. Help toward this goal might come from AC-LEDs introduced in the market in 2012. They are devoid of transformer, which improves their efficiency (claims up to 85% power efficiency has been filed). To compensate the flickering due to alternative electro-excitation, phosphors with long lifetimes (long persistence phosphors) are used that contain $Eu^{II/III}$ and Tb^{III}. It is however presently too early to predict if AC-LEDs are really going to supplant conventional LEDs in view of the large improvements achieved recently in the latter.

5.4 Displays

The phosphors of cathode-ray tube displays commercialized in the mid-1950s were very similar to those of fluorescent tubes. These tubes were then replaced with flat-panel displays based on several different technologies,

liquid crystals, plasma and electroluminescent panels, or, lately, organic LEDs. Except for the latter, most of these panels still work on the RGB principle, and a combination of older and newer RE-containing phosphors makes them shine brightly. The market is evolving rapidly, especially with the spread of smart phones and tablets on one hand and with new emerging technologies sometimes replacing rare-earth phosphors, so that it is difficult to predict the fate of these phosphors, except that it seems that red-emitting Eu^{III} will keep a privileged share in this market.

5.5 Security and Signage

5.5.1 The Tools

The well-defined emission bands of lanthanide luminescence and the possibility of designing fingerprints (or bar codes) by mixing several lanthanides in a probe have prompted its use in security inks, counterfeiting tags, and safety signage, not to mention pressure sensors or luminescent toys.

Several of these applications are based on downshifted luminescence, that is, emission in the visible/NIR following excitation in the UV/visible.

A very important development has been the discovery in 1966 by F. Auzel that anti-Stokes luminescence could be generated by energy transfer between two excited ions leading to upconversion [68]. In this process, two or more long-wavelength photons are combined into a shorter wavelength one. Several mechanisms are operative, in particular, excited-state absorption or energy transfer upconversion with the help of a sensitizer. Corresponding materials are usually inorganic, e.g., the ubiquitous hexagonal $NaYF_4$:Yb(18–20%)Ln (x%), Ln = Er ($x = 2$), Tm ($x = 0.5$). Trivalent erbium emits around 540 (green) and 650 nm (red), while Tm^{III} has emission at 290, 350, 460, 660 (weak), and 800 nm. In order to make these materials more compatible with practical applications, they are commonly used under the form of nanoparticles, the surface of which can be easily derivatized. Upconversion nanoparticles (UCNPs) are now ubiquitous in many applications, including luminescent tags, biosciences, drug delivery, photocatalysis, or solar energy conversion. Quantum yields of upconversion are often low, because the phenomenon is a multiphoton process and this is worsened in UCNPs in view of enhanced nonradiative deactivation due to surface traps and defects that increase with decreasing size. The remedy is to design core-shell UCNPs in which the active core material is coated with a nonluminescent layer of the matrix, passivating surface defects. The field has sustained hefty developments lately that led to remarkable control of the emissive properties. The red-to-green Er^{III} intensity ratio can be tuned by surface modification, adjusting the composition (e.g., by co-doping Mn^{II} or Gd^{III} ions) or the size/structure of the NPs. Increasing the brightness of UCNPs has also been a constant preoccupation, and excellent results have been obtained, by linking UCNPs with silver or

gold islets and taking advantage of plasmon resonances, with enhancement factors reaching 300-fold [69], by modifying their composition [69], by elaborating multi-shell NPs [70], or by 3D-controlled growth [71]. Presently, quantum yields up to several percent are achievable, for instance, with the $LiLuF_4$:Ln system: 5% for Er and 7.6% for Tm [72].

5.5.2 Security Inks

Some of the security features implemented in banknotes rely on lanthanide luminescence. For instance, the orange–red luminescence of euro banknotes under UV excitation clearly arises from a Eu^{III} compound, while the bluish-greenish emission could be due to a Eu^{II} pigment (Fig. 12A). Downshifted luminescence is also used in printing secret documents or counterfeiting tags so that text or pictures can only be revealed under UV illumination [73].

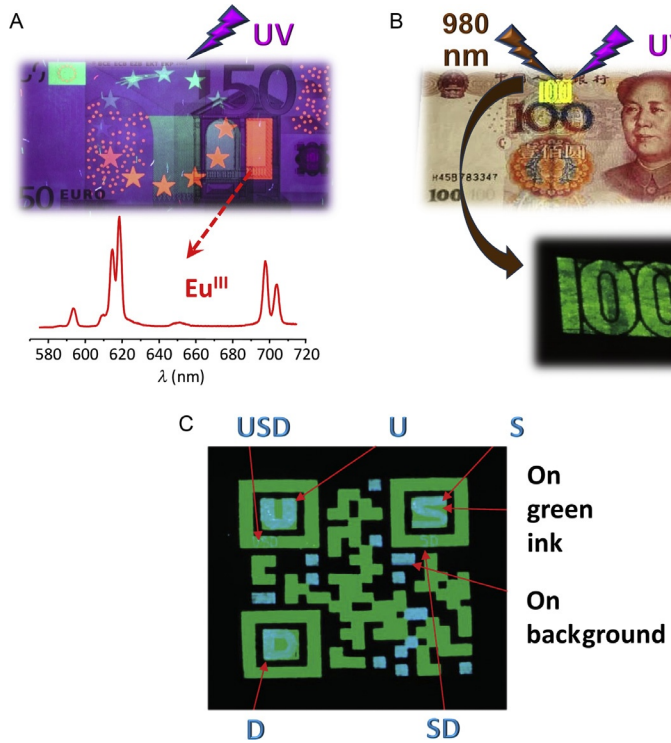

FIG. 12 (A) 50-euro banknote under UV light; (B) 100-yuan banknote under UV and NIR illumination; (C) QR code under 980-nm illumination: emission from $NaYF_4$:Yb(20%),Ln(2%), Ln = Er (*green*, 540 nm), Tm (*blue*, 450–470 nm). *Panel (B): Courtesy of Prof. Liu Xiaogang, NUS, Singapore. Panel (C): Redrawn from J.M. Meruga, W.M. Cross, P.S. May, Q.A. Luu, G.A. Crawford, J.J. Kellar, Security printing of covert quick response codes using upconverting nanoparticle inks, Nanotechnology 23 (2012) Art. Nr. 395201.*

Similarly, banknotes from China include a rectangular spot that emits yellow light under UV excitation. But when this spot is illuminated with 980-nm light, an upconverted green luminescent number is revealed that corresponds to the face value of the banknote (Fig. 12B). Quite spectacular too is the "secret" information that can be embedded into bar codes or quick-response (QR) codes (Fig. 12C) thanks to UCNPs. Similar features are incorporated in identity documents as well as in marking and counterfeiting tags.

5.5.3 Bar Codes for Tagging Commercial Goods

Counterfeiting has emerged as being a major problem for brand marks. Combining several lanthanide ions into one phosphor material leads to designing bar codes or recognition/counterfeiting tags [74]. Several companies are selling rare earth-containing tags for marking batches of various goods as diverse as clothes, airplane fuels, or ammunition. Regarding the latter, explosion transforms the tags into a mixture of rare-earth oxides that retain the same composition as the initial tag, allowing tracing the origin of the ammunition or explosive powder. Similarly, epitaxial growth of hexagonal nanorods encompassing different $NaYF_4$:Yb,Ln phosphors allow designing different RGB combinations for specific nanomarking [75]. Counterfeiting tags take advantage not only of the spectral signature of luminescent lanthanide mixtures but, also, of their different lifetimes.

5.5.4 Safety Signage

Persistent luminescence is the property of some luminescent materials to continue to emit light long after the excitation source is switched off. Zinc sulfide doped with transition metals, for instance, copper and cobalt, has long been used in conjunction with ^{226}Ra as excitation source in luminous paints for watch and clock dials. An important step was achieved in 1994 when it was found that co-doping Eu^{II} and Dy^{III} into strontium aluminate, $SrAl_2O_4$:Eu^{II}, Dy^{III}, resulted in a brighter phosphor that increasingly replaced the historical zinc sulfide materials. Applications as diverse as safety signage (e.g., luminous strips indicating emergency issues) or luminous toys are now standard. Less convincing is road marking (a test has been made in The Netherlands in 2014 with limited success) or energy storage (for solar cells, but the capacity is rather small) [11].

5.6 Life Sciences and Medicine [76–78]

Since the mid-1970s, lanthanide luminescence bioprobes (LLBs) are used in time-resolved luminescent immunoassays, the sensitivity of which is comparable and even better than that of radioactivity-based assays. Applications to bioimaging [78] and drug release [17] have been slower to develop, but they are presently on an upward trend. Both lanthanide complexes and inorganic

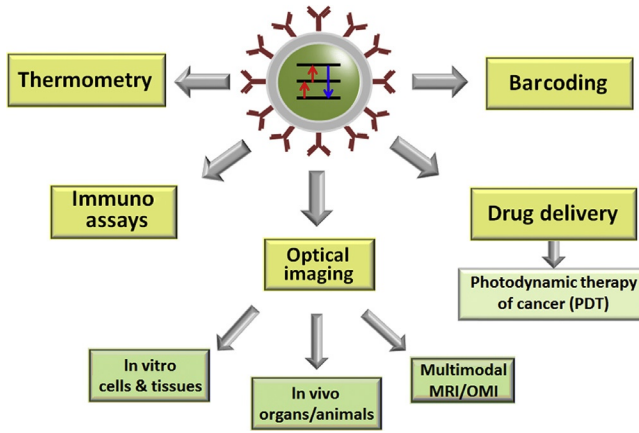

FIG. 13 Applications of UCNPs in biosciences. *Reproduced with permission from J.-C.G. Bünzli, Lanthanide light for biology and medical diagnosis, J. Lumin. 170 (2016) 866–878, © 2016 Elsevier Science B.V.*

compounds (particularly UCNPs) are used, often conjugated to avidin, biotin, monoclonal antibodies, or peptides, to ensure biochemical specificity. Interest is large because several features of lanthanide luminescence are unique, rendering LLBs quite competitive with respect to other conventional probes:

- narrow emission bands and large ligand-induced Stokes shifts
- long lifetimes allowing time-gated detection
- little (complexes with organic ligands) or no (inorganic probes) photobleaching
- easy multiplexing experiments when combining several Ln probes
- possibility of designing NIR–NIR imaging systems [79].

The field has been over-reviewed during the past years, particularly with respect to UCNP-based bioprobes [80] so that we do not elaborate further here, leaving the readers consulting relevant literature entries. As an example though, Fig. 13 sketches the various applications of UCNPs in biosciences. It is noteworthy that recent progresses in Ln-based luminescent thermometry allow for measuring temperature within cells [20]. In addition, lanthanide-based optical encoding materials enable multiplexing of large numbers of samples including assays involving nucleic acids or protein–antibody pairs, as well as multiplexed immunohistochemical staining of cells and tissues (Parallume® technology).

5.7 Scintillators

Radiation detection is important to several fields, including defense, medicine (e.g., PET, CT scans), material testing, environmental hazard monitoring, or

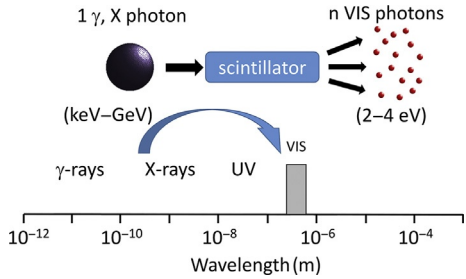

FIG. 14 Wavelength conversion by a scintillator.

security checks at harbors, airports, and borders. It turns out that there is no direct sensitive detector for photons with energy larger than a few keV. A wavelength-converting material is therefore needed (Fig. 14). Earlier scintillator crystals were often made of simple lanthanide salts, such as lanthanum or cerium chloride or bromide, or of calcium fluoride doped with divalent europium. More efficient ones are now at hand, featuring various inorganic matrices such as lutetium silicate, aluminate, or halides doped with Ce^{III} [81]. Present record is held by $Lu_3Al_5O_{12}$:Ce with a yield of 25,000 photons per MeV [82].

5.8 Solar Energy Conversion and Photocatalysis

The role of wavelength-converting lanthanides in solar energy conversion has been the subject of a recent chapter in this series [21]. Converting UV light into visible light improves the yield by 1–2 absolute% in Si-based cells and by 1.5 absolute% in dye-sensitized cells. Converting NIR light is much more difficult since sun illumination has low power density (0.1 W cm^{-2}), resulting in very low upconversion yields; for the time being, improvement around only 0.5 absolute% has been demonstrated. With the progress of nanotechnology, particularly nanopatterning, one may expect that this figure will double or triple in the forthcoming years and that combining downshifting, upconversion, and other effects could lead to a total increase in the yield between 4 and 5 absolute%. Whether implementation of the corresponding wavelength-converting layers will be cost competitive remains to be seen.

Cerium oxide or anatase (TiO_2) doped with Ce^{III} ions is an efficient photocatalyst for water splitting under UV excitation. One goal though is to gain photocatalytic activity under sun illumination alone and UCNPs can help. For instance, Tm-based UCNPs coated with TiO_2 produce UV and blue light under IR solar irradiation that activates TiO_2 photocatalytic properties for air and water purification [83]. Moreover, thermal reduction of ceria in an aerosol reactor illuminated by concentrated solar light promotes the splitting of both water and carbon dioxide, producing syngas that is ultimately transformed into kerosene with solar-to-kerosene yield of 1.7% [84]. These applications are still confined to research laboratories but may develop into economical processes.

Another interesting use of solar irradiation lies in plastics for agriculture that are doped with lanthanide-containing (mainly Eu^{III}) salts or complexes. The resulting emission matches well the photosynthesis efficiency curve, and improvement in crop yields of 10% can be routinely achieved, which is important in view of the growing world population.

6 WHAT IS NEXT?

As for any other rare-earth applications, lanthanide photonics is subject to large market oscillations due to extreme price variations on one hand (caused by geopolitical factors) and to evolving technologies on the other hand. When a technology becomes obsolete, it is replaced by another, more performing one, possibly cheaper, but which does not necessarily need the same amount of rare earth, if any at all. The case of phosphors is quite typical. Present demand for the classical RGB phosphors is plummeting owing to the replacement of compact fluorescent lamps with LEDs, and prices have declined by 60% during the past 2 years. On the other hand, several phosphors for LEDs still contain lanthanides, particularly the red phosphor, though in smaller quantities, and their commercial growth rate is predicted to reach 30% during the next 5 years. Similar phosphors are also provided in all kind of displays, particularly in back lighting of liquid crystal displays. As a consequence, research in this field will continue to be very active, particularly when it comes to nanopatterning in order to better modulate the photophysical properties and to increase the luminance.

Among the fast developing applications are biosensing, bioimaging, and luminescent thermometry. Here, the potential of lanthanide luminescent (bio)probes, including UCNPs, begins only to be explored and deep progresses are predicted. When it comes to UCNPs, present work is concentrating on improving their performances, particularly the quantum yield and luminosity, through clever design of sophisticated nanostructures. Understanding the exact mechanism of energy migration and conversion in these complicated systems will certainly help progressing further. Moreover, a breakthrough has been reached in 2012 for molecular upconversion demonstrated at low temperature in a trinuclear bimetallic Cr–Er–Cr helicate [85]. Molecular upconversion has now been demonstrated to occur at room temperature [86], and this provides another whopping handle to optimize light upconversion by modifying the structure of the ligands.

Solar energy conversion is a stimulating field, and much is needed to succeed in designing commercially viable wavelength-converting layers. But again, materials improvements are at hand, as well as new photonic tricks (photonic crystals, solar concentrators, combination of quantum dots with wavelength-converting layers) that should contribute bringing this field closer to practical use.

New exciting results are presently being found in two futuristic disciplines that have recently been reviewed: optical refrigeration [22] and quantum

information processing, leading to much desired optical computing [23]. These fields need not only materials development but also theoretical modeling, much as energy transfer processes in complexes with organic ligands.

As a conclusion, lanthanide photonics is a science in full development and will provide jewels in many different domains including health sciences, safety procedures, and green energy production. Its future is bright!

ABBREVIATIONS AND SYMBOLS

CT	charge transfer
ED	electric dipole
EDFA	erbium-doped fiber amplifier
EQ	electric quadrupole
HS	high spin
JO	Judd–Ofelt
LED	light-emitting diode
LF	ligand field
LMCT	ligand-to-metal charge transfer
MD	magnetic dipole
MLCT	metal-to-ligand charge transfer
MMCT	metal-to-metal charge transfer
NIR	near-infrared
RGB	red–green–blue
UCNP	upconversion nanoparticle
UV	ultraviolet
WLED	white light-emitting diode
YAG	yttrium aluminum garnet, $Y_3Al_5O_{12}$

REFERENCES

[1] J.-C.G. Bünzli, On the design of highly luminescent lanthanide complexes, Coord. Chem. Rev. 293–294 (2015) 19–47.

[2] J.-C.G. Bünzli, S.V. Eliseeva, Intriguing aspects of lanthanide luminescence, Chem. Sci. 4 (2013) 1939–1949.

[3] I. Hernandez, W.P. Gillin, Organic chromophores-based sensitization of NIR-emitting lanthanides: toward highly efficient halogenated environments, in: J.-C.G. Bünzli, V.K. Pecharsky (Eds.), Handbook on the Physics and Chemistry of Rare Earths, vol. 47, Elsevier Science B.V., Amsterdam, 2015, pp. 1–100. Chapter 269.

[4] S. Comby, J.-C.G. Bünzli, Lanthanide near-infrared luminescence in molecular probes and devices, in: K.A. Gschneidner Jr., J.-C.G. Bünzli, V.K. Pecharsky (Eds.), Handbook on the Physics and Chemistry of Rare Earths, vol. 37, Elsevier Science B.V., Amsterdam, 2007, pp. 217–470. Chapter 235.

[5] N. Sabbatini, M. Guardigli, I. Manet, Antenna effect in encapsulation complexes of lanthanide ions, in: K.A. Gschneidner Jr., L. Eyring (Eds.), Handbook on the Physics and Chemistry of Rare Earths, vol. 23, Elsevier Science B.V., Amsterdam, 1996, pp. 69–120. Chapter 154.

[6] W.T. Carnall, The absorption and fluorescence spectra of rare earth ions in solution, in: K.A. Gschneidner Jr., L. Eyring (Eds.), Handbook on the Physics and Chemistry of Rare Earths, vol. 3, North Holland, Amsterdam, 1979, pp. 171–208. Chapter 24.
[7] F. Auzel, Coherent emission in rare-earth materials, in: K.A. Gschneidner Jr., L. Eyring (Eds.), Handbook on the Physics and Chemistry of Rare Earths, vol. 22, Elsevier Science Publ. B.V., Amsterdam, 1996, pp. 507–606. Chapter 151.
[8] W.M. Yen, Laser spectroscopy, in: K.A. Gschneidner Jr., J.-C.G. Bünzli, V.K. Pecharsky (Eds.), Handbook on the Physics and Chemistry of Rare Earths, vol. 12, Elsevier Science B.V., Amsterdam, 1989, pp. 433–477. Chapter 87.
[9] R. Reisfeld, C.K. Jorgensen, Excited state phenomena in vitreous materials, in: K.A. Gschneidner Jr., L. Eyring (Eds.), Handbook on the Physics and Chemistry of Rare Earths, vol. 9, Elsevier Science Publ. B.V., Amsterdam, 1987, pp. 1–90. Chapter 58.
[10] A. Halperin, Activated thermoluminescence (TL) dosimeters and related radiation detectors, in: K.A. Gschneidner Jr., L. Eyring (Eds.), Handbook on the Physics and Chemistry of Rare Earths, vol. 28, Elsevier B.V., Amsterdam, 2000, pp. 187–309. Chapter 179.
[11] P.F. Smet, K. Van den Eeckhout, O.Q. De Clercq, D. Poelman, Persistent phosphors, in: J.-C.G. Bünzli, V.K. Pecharsky (Eds.), Handbook on the Physics and Chemistry of Rare Earths, vol. 48, Elsevier Science B.V., Amsterdam, 2015, pp. 1–108. Chapter 274.
[12] A.J. Freeman, B.I. Min, M.R. Norman, Local density supercell theory of photoemission and inverse photoemission spectra, in: K.A. Gschneidner Jr., L. Eyring, S. Hüfner (Eds.), Handbook on the Physics and Chemistry of Rare Earths, vol. 10, Elsevier Science Publishers B.V., Amsterdam, 1987, pp. 165–229. Chapter 65.
[13] D.W. Lynch, J.H. Weaver, Photoemission of Ce and its compounds, in: K.A. Gschneidner Jr., L. Eyring, S. Hüfner (Eds.), Handbook on the Physics and Chemistry of Rare Earths, vol. 10, Elsevier B.V., Amsterdam, 1987, pp. 231–300. Chapter 66.
[14] S. Hüfner, Photoemission in chalcogenides, in: K.A. Gschneidner Jr., L. Eyring, S. Hüfner (Eds.), Handbook on the Physics and Chemistry of Rare Earths, vol. 10, Elsevier Science Publishers B.V., Amsterdam, 1987, pp. 301–319. Chapter 67.
[15] S. Shinoda, H. Miyake, H. Tsukube, Molecular recognition and sensing via rare earth complexes, in: K.A. Gschneidner Jr., J.-C.G. Bünzli, V.K. Pecharsky (Eds.), Handbook on the Physics and Chemistry of Rare Earths, vol. 35, Elsevier Science B.V., Amsterdam, 2005, pp. 273–331. Chapter 226.
[16] T. Nishioka, K. Fukui, K. Matsumoto, Lanthanide chelates as luminescent labels in biomedical analyses, in: K.A. Gschneidner Jr., J.-C.G. Bünzli, V.K. Pecharsky (Eds.), Handbook on the Physics and Chemistry of Rare Earths, vol. 37, Elsevier Science B.V., Amsterdam, 2007, pp. 171–216. Chapter 234.
[17] D.C. Rodriguez Burbano, R. Naccache, J.A. Capobianco, Near-IR triggered photon upconversion: imaging, detection, and therapy, in: J.-C.G. Bünzli, V.K. Pecharsky (Eds.), Handbook on the Physics and Chemistry of Rare Earths, vol. 47, Elsevier Science B.V., Amsterdam, 2015, pp. 273–347. Chapter 273.
[18] G.K. Liu, X.Y. Chen, Spectroscopic properties of lanthanides in nanomaterials, in: K.A. Gschneidner Jr., J.-C.G. Bünzli, V.K. Pecharsky (Eds.), Handbook on the Physics and Chemistry of Rare Earths, vol. 37, Elsevier Science B.V., Amsterdam, 2007, pp. 99–169. Chapter 233.
[19] M. Sato, S.W. Kim, Y. Shimomura, T. Hasegawa, K. Toda, G.Y. Adachi, Rare earth-doped phosphors for white light-emitting diodes, in: J.-C.G. Bünzli, V.K. Pecharsky (Eds.), Handbook on the Physics and Chemistry of Rare Earths, vol. 49, Elsevier Science B.V., Amsterdam, 2016, pp. 1–128. Chapter 278.

[20] C.D.S. Brites, A. Millan, L.D. Carlos, Lanthanides in luminescent thermometry, in: J.-C.G. Bünzli, V.K. Pecharsky (Eds.), Handbook on the Physics and Chemistry of Rare Earths, vol. 49, Elsevier Science B.V., Amsterdam, 2016, pp. 339–427. Chapter 281.
[21] J.-C.G. Bünzli, A.-S. Chauvin, Lanthanides in solar energy conversion, in: J.-C.G. Bünzli, V. K. Pecharsky (Eds.), Handbook on the Physics and Chemistry of Rare Earths, vol. 44, Elsevier Science B.V., Amsterdam, 2014, pp. 169–281. Chapter 261.
[22] M.P. Hehlen, M. Sheik-Bahae, R.I. Epstein, Solid-state optical refrigeration, in: J.-C.G.Bünzli, V.K. Pecharsky (Eds.), Handbook on the Physics and Chemistry of Rare Earths, vol. 45, Elsevier Science B.V., Amsterdam, 2014, pp. 179–260. Chapter 265.
[23] P. Goldner, A. Ferrier, O. Guillot-Noël, Rare-earth doped crystal for quantum information processing, in: J.-C.G. Bünzli, V.K. Pecharsky (Eds.), Handbook on the Physics and Chemistry of Rare Earths, vol. 46, Elsevier Science B.V., Amsterdam, 2015, pp. 1–78. Chapter 267.
[24] C. Görller-Walrand, K. Binnemans, Spectral intensities of f-f transitions, in: K.A. Gschneidner Jr., L. Eyring (Eds.), Handbook on the Physics and Chemistry of Rare Earths, vol. 25, Elsevier Science B.V., Amsterdam, 1998, pp. 101–264. Chapter 167.
[25] M. Dolg, H. Stoll, Electronic structure calculations for molecules containing lanthanide atoms, in: K.A. Gschneidner Jr., E.M. Eyring (Eds.), Handbook on the Physics and Chemistry of Rare Earths, vol. 22, Elsevier Science B.V., Amsterdam, 1996, pp. 607–720. Chapter 152.
[26] K. Ogasawara, S. Watanabe, H. Toyoshima, M.G. Brik, First-principles calculations of 4f-4f5d transition spectra, in: K.A. Gschneidner Jr., J.-C.G. Bünzli, V.K. Pecharsky (Eds.), Handbook on the Physics and Chemistry of Rare Earths, vol. 37, Elsevier Science B.V., Amsterdam, 2007, pp. 1–59. Chapter 231.
[27] E.N. Harvey, A History of Luminescence. From the Earliest Times Until 1900, American Philosophical Society, Philadelphia, 1957.
[28] G. Urbain, Twenty-five years of research on the yttrium earths, Chem. Rev. 1 (1924) 143–185.
[29] J.H. Van Vleck, The puzzle of rare-earth spectra in solids, J. Phys. Chem. 41 (1937) 67–80.
[30] H. Bethe, Termaufspaltung in Kristallen, Ann. Phys. 395 (1929) 133–208.
[31] P. Dorenbos, The 4f to 4f5d transitions of the trivalent lanthanides in halogenides and chalcogenides, J. Lumin. 91 (2000) 91–106.
[32] B.G. Wybourne, Spectroscopic Properties of Rare Earths, Wiley Interscience, New York, 1965.
[33] G.H. Dieke, Spectra and Energy Levels of Rare Earth Ions in Crystals, Interscience Publishers, New York, 1968.
[34] C. Görller-Walrand, K. Binnemans, Rationalization of crystal field parameterization, in: K. A. Gschneidner Jr., L. Eyring (Eds.), Handbook on the Physics and Chemistry of Rare Earths, vol. 23, Elsevier Science B.V., Amsterdam, 1996, pp. 121–283. Chapter 155.
[35] B.M. Walsh, Judd Ofelt theory: principles and practices, in: B. Di Bartolo, O. Forte (Eds.), Advances in Spectroscopy for Lasers and Sensing, Springer Verlag, Berlin, 2006, pp. 403–433.
[36] A. Meijerink, R.T. Wegh, VUV spectroscopy of lanthanides: extending the horizon, Mater. Sci. Forum 315–317 (1999) 11–26.
[37] L. van Pieterson, M.F. Reid, R.T. Wegh, A. Meijerink, 4f(n) <-> 4f(n-1)5d transitions of the trivalent lanthanides: experiment and theory, J. Lumin. 94 (2001) 79–83.
[38] L. Brewer, Systematics of the properties of the lanthanides, in: S.P. Sinha (Ed.), Systematics and the Properties of the Lanthanides, Springer Verlag, Berlin, 1983, pp. 17–69.

[39] L. van Pieterson, M.F. Reid, G.W. Burdick, A. Meijerink, 4f(n)->4f(n-1)5d transitions of the heavy lanthanides: experiment and theory, Phys. Rev. B 65 (2002). Art. Nr. 045114-1–045114-13.
[40] L. van Pieterson, M.F. Reid, R.T. Wegh, S. Soverna, A. Meijerink, 4f(n)->4f(n-1)5d transitions of the light lanthanides: experiment and theory, Phys. Rev. B 65 (2002). Art. Nr. 045113-1–045113-16.
[41] P. Dorenbos, Predictability of 5d level positions of the triply ionized lanthanides in halogenides and chalcogenides, J. Lumin. 87–89 (2000) 970–972.
[42] A. Zych, J. Ogieglo, C. Ronda, D.C. de Mello, A. Meijerink, Analysis of the shift of zero-phonon lines for f-d luminescence of lanthanides in relation to the Dorenbos model, J. Lumin. 134 (2013) 174–179.
[43] J.-C.G. Bünzli, S.V. Eliseeva, Basics of lanthanide photophysics, in: O.S. Wolfbeis, M. Hof (Eds.), Lanthanide Luminescence: Photophysical, Analytical and Biological Aspects, Springer Series on Fluorescence, vol. 7, Springer Verlag, Berlin, 2011, pp. 1–45.
[44] J.-C.G. Bünzli, S.V. Eliseeva, Photophysics of lanthanoid coordination compounds, in: V. W.-W. Yam (Ed.), Comprehensive Inorganic Chemistry II, Elsevier B.V., Amsterdam, 2013, pp. 339–398.
[45] P.A. Tanner, Some misconceptions concerning the electronic spectra of tri-positive europium and cerium, Chem. Soc. Rev. 42 (2013) 5090–5101.
[46] J.-C.G. Bünzli, Luminescent probes, in: J.-C.G. Bünzli, G.R. Choppin (Eds.), Lanthanide Probes in Life, Chemical and Earth Sciences. Theory and Practice, Elsevier Science Publ. B.V., Amsterdam, 1989, pp. 219–293
[47] M.H.V. Werts, R.T.F. Jukes, J.W. Verhoeven, The emission spectrum and the radiative lifetime of Eu^{3+} in luminescent lanthanide complexes, Phys. Chem. Chem. Phys. 4 (2002) 1542–1548.
[48] H. Kunkely, A. Vogler, Photolysis of aqueous europium(III) azide complexes: formation of europium(II) induced by ligand-to-metal charge transfer excitation, Inorg. Chem. Commun. 8 (2005) 117–118.
[49] L.D. Carlos, J.A. Fernandes, R.A.S. Ferreira, O.L. Malta, I.S. Goncalves, P. Ribeiro-Claro, Emission quantum yield of a europium(III) tris-beta-diketonate complex bearing a 1,4-diaza-1,3-butadiene: comparison with theoretical prediction, Chem. Phys. Lett. 413 (2005) 22–24.
[50] J.-C.G. Bünzli, P. Froidevaux, J.M. Harrowfield, Photophysical properties of lanthanide dinuclear complexes with p-tert-butylcalix[8]arene, Inorg. Chem. 32 (1993) 3306–3311.
[51] J.-C.G. Bünzli, F. Ihringer, Photophysical properties of lanthanide dinuclear complexes with p-nitro-calix[8]arene, Inorg. Chim. Acta 246 (1996) 195–205.
[52] A. D'Aleo, F. Pointillart, L. Ouahab, C. Andraud, O. Maury, Charge transfer excited states sensitization of lanthanide emitting from the visible to the near-infra-red, Coord. Chem. Rev. 256 (2012) 1604–1620.
[53] F.F. Chen, Z.Q. Chen, Z.Q. Bian, C.H. Huang, Sensitized luminescence from lanthanides in d-f bimetallic complexes, Coord. Chem. Rev. 254 (2010) 991–1010.
[54] M.D. Ward, Mechanisms of sensitization of lanthanide(III)-based luminescence in transition metal/lanthanide and anthracene/lanthanide dyads, Coord. Chem. Rev. 254 (2010) 2634–2642.
[55] S.I. Weissman, Intramolecular energy transfer. The luminescence of complexes of europium (β-diketonate complexes), J. Chem. Phys. 10 (1942) 214–217.
[56] Th. Förster, Zwischenmolekulare Energiewanderung und Fluoreszenz, Ann. Phys. 2 (1948) 55–75.
[57] D.L. Dexter, A theory of sensitized luminescence in solids, J. Chem. Phys. 21 (1953) 836–850.

[58] W.R. Liu, P.C. Lin, A study on luminescence properties and energy transfer mechanism for NaCaY(PO4)2:Eu2+, Mn2+ phosphors for LED applications, Opt. Express 22 (2014) A446–A451.
[59] M. Kleinerman, Energy migration in lanthanide chelates, J. Chem. Phys. 51 (1969) 2370–2381.
[60] L.N. Puntus, K.A. Lyssenko, I. Pekareva, J.-C.G. Bünzli, Intermolecular interactions as actors in energy transfer processes in lanthanide complexes with 2,2'-bipyridine, J. Phys. Chem. B 113 (2009) 9265–9277.
[61] Y. Zhang, P.C. Jiao, H.B. Xu, M.J. Tang, X.P. Yang, S. Huang, J.G. Deng, Switchable sensitizers stepwise lighting up lanthanide emissions, Sci. Rep. 5 (2015). Art. Nr. 9335-1–9335-5.
[62] G.F. de Sá, O.L. Malta, C.D. Donega, A.M. Simas, R.L. Longo, P.A. Santa-Cruz, E.F. da Silva, Spectroscopic properties and design of highly luminescent lanthanide coordination complexes, Coord. Chem. Rev. 196 (2000) 165–195. review.
[63] G.B. Rocha, R.O. Freire, N.B. Da Costa, G.F. de Sá, A.M. Simas, Sparkle model for AM1 calculation of lanthanide complexes: improved parameters for europium, Inorg. Chem. 43 (2004) 2346–2354.
[64] M.A.M. Filho, J.D.L. Dutra, H.L.B. Cavalcanti, G.B. Rocha, A.M. Simas, R.O. Freire, RM1 model for the prediction of geometries of complexes of the trications of Eu, Gd, and Tb, J. Chem. Theory Comput. 10 (2014) 3031–3037.
[65] S. Biju, R.O. Freire, Y.K. Eom, R. Scopelliti, J.-C.G. Bünzli, H.K. Kim, A Eu(III) tetrakis (b-diketonate) dimeric complex: photophysical properties, structural elucidation by sparkle/AM1 calculations, and doping into PMMA films and nanowires, Inorg. Chem. 53 (2014) 8407–8417.
[66] S.V. Eliseeva, J.-C.G. Bünzli, Rare earths: jewels for functional materials of the future, New J. Chem. 35 (2011) 1165–1176.
[67] V. Tucureanu, A. Matei, A.M. Avram, Synthesis and characterization of YAG:Ce phosphors for white LEDs, Opto-Electron. Rev. 23 (2015) 239–251.
[68] F. Auzel, Upconversion and anti-stokes processes with f and d ions in solids, Chem. Rev. 104 (2004) 139–173.
[69] S.Y. Han, R.R. Deng, X.J. Xie, X.G. Liu, Enhancing luminescence in lanthanide-doped upconversion nanoparticles, Angew. Chem. Int. Ed. 53 (2014) 11702–11715.
[70] H.L. Wen, H. Zhu, X. Chen, T.F. Hung, B.L. Wang, G.Y. Zhu, S.F. Yu, F. Wang, Upconverting near-infrared light through energy management in core-shell-shell nanoparticles, Angew. Chem. Int. Ed. 52 (2013) 13419–13423.
[71] D. Liu, X. Xu, Y. Du, X. Qin, Y. Zhang, C. Ma, S. Wen, W. Ren, E.M. Goldys, J.A. Piper, S. Dou, X. Liu, D. Jin, Three-dimensional controlled growth of monodisperse sub-50 nm heterogeneous nanocrystals, Nat. Commun. 7 (2016). Art. Nr. 10254-1–10254-8.
[72] P. Huang, W. Zheng, S.Y. Zhou, D.T. Tu, Z. Chen, H.M. Zhu, R.F. Li, E. Ma, M.D. Huang, X.Y. Chen, Lanthanide-doped LiLuF4 upconversion nanoprobes for the detection of disease biomarkers, Angew. Chem. Int. Ed. 53 (2014) 1252–1257.
[73] J. Andres, R.D. Hersch, J.E. Moser, A.S. Chauvin, A new anti-counterfeiting feature relying on invisible luminescent full color images printed with lanthanide-based inks, Adv. Funct. Mater. 24 (2014) 5029–5036.
[74] O. Guillou, C. Daiguebonne, G. Calvez, K. Bernot, A long journey in lanthanide chemistry: from fundamental crystallogenesis studies to commercial anticounterfeiting taggants, Acc. Chem. Res. 49 (2016) 844–856.
[75] Y. Zhang, L. Zhang, R. Deng, J. Tian, Y. Zong, D. Jin, X. Liu, Multicolor barcoding in a single upconversion crystal, J. Am. Chem. Soc. 136 (2014) 4893–4896.

[76] J.-C.G. Bünzli, Lanthanide luminescence for biomedical analyses and imaging, Chem. Rev. 110 (2010) 2729–2755.
[77] J.-C.G. Bünzli, Lanthanide light for biology and medical diagnosis, J. Lumin. 170 (2016) 866–878.
[78] J.-C.G. Bünzli, Luminescence bioimaging with lanthanide complexes, in: A. de Bettencourt-Dias (Ed.), Luminescence in Lanthanide Coordination Compounds and Nanomaterials, Wiley-Blackwell, Oxford, 2014, pp. 125–197.
[79] E. Hemmer, N. Venkatachalam, H. Hyodo, A. Hattori, Y. Ebina, H. Kishimoto, K. Soga, Upconverting and NIR emitting rare earth based nanostructures for NIR-bioimaging, Nanoscale 5 (2013) 11339–11361.
[80] Z. Chen, W. Zheng, P. Huang, D. Tu, S. Zhou, M. Huang, X. Chen, Lanthanide-doped luminescent nano-bioprobes for the detection of tumor markers, Nanoscale 7 (2015) 4274–4290.
[81] M. Nikl, A. Yoshikawa, Recent R&D trends in inorganic single-crystal scintillator materials for radiation detection, Adv. Opt. Mater. 3 (2015) 463–481.
[82] S. Liu, J.A. Mares, X. Feng, A. Vedda, M. Fasoli, Y. Shi, H. Kou, A. Beitlerova, L. Wu, C. D'Ambrosio, Y. Pan, M. Nikl, Towards bright and fast Lu3Al5O12:Ce, Mg optical ceramics scintillators, Adv. Opt. Mater. 4 (2016) 731–739.
[83] X. Guo, W. Di, C. Chen, C. Liu, X. Wang, W. Qin, Enhanced near-infrared photocatalysis of NaYF4:Yb, Tm/CdS/TiO2 composites, Dalton Trans. 43 (2014) 1048–1054.
[84] J.R. Scheffe, M. Welte, A. Steinfeld, Thermal reduction of ceria within an aerosol reactor for H_2O and CO_2 splitting, Ind. Eng. Chem. Res. 53 (2014) 2175–2182.
[85] J.F. Lemonnier, L. Babel, L. Guenee, P. Mukherjee, D.H. Waldeck, S.V. Eliseeva, S. Petoud, C. Piguet, Perfluorinated aromatic spacers for sensitizing europium(III) centers in dinuclear oligomers: better than the best by chemical design? Angew. Chem. Int. Ed. 51 (2012) 11302–11305.
[86] A. Nonat, C.F. Chan, T. Liu, C. Platas-Iglesias, Z. Liu, W.T. Wong, W.K. Wong, K.L. Wong, L.J. Charbonniere, Room temperature molecular up conversion in solution, Nat. Commun. 7 (2016). Art. Nr. 111978-1–111978-8.